Field-Free-Switching State Diagram of Perpendicular Magnetization Subjected to Conventional and Unconventional Spin-Orbit Torques

D.J.P. de Sousa,[1,*] P.M. Haney,[2] J.P. Wang,[1] and Tony Low[1,†]

[1]*Department of Electrical and Computer Engineering, University of Minnesota, Minneapolis, Minnesota 55455, USA*

[2]*Physical Measurement Laboratory, National Institute of Standards and Technology, Gaithersburg, Maryland 20899-6202, USA*

The lack of certain crystalline symmetries in strong spin-orbit-coupled nonmagnetic materials allows for the existence of unconventional spin Hall responses, with electrically generated transverse spin currents possessing collinear flow and spin directions. The injection of such spin currents into an adjacent ferromagnetic layer can excite magnetization dynamics via unconventional spin-orbit torques, leading to deterministic switching in ferromagnets with perpendicular magnetic anisotropy. We study the interplay between conventional and unconventional spin-orbit torques on the magnetization dynamics of a perpendicular ferromagnet in the small intrinsic damping limit, and identify a rich set of dynamical regimes that includes deterministic and probabilistic switching, precessional and pinning states. Contrary to common belief, we find that there exists a critical conventional spin Hall angle, beyond which deterministic magnetization switching transitions to a precessional or pinned state. Conversely, we show that larger unconventional spin Hall angle is generally beneficial for deterministic switching. We derive an approximate expression that qualitatively describes the state-diagram boundary between the full deterministic switching and precessional states and discuss a criterion for searching symmetry-broken spin Hall materials in order to maximize switching efficiency. Our work offers a roadmap towards energy-efficient spintronic devices, which might open the door for applications in advanced in-memory computing technologies.

I. INTRODUCTION

Energy-efficient, external magnetic field-free switching of a thin ferromagnetic film with perpendicular magnetic anistropy (PMA) is highly desirable for alternative applications in magnetic based memories and in-memory computing technologies [1–6]. Modern approaches to induce field-free switching in PMA ferromagnets (FMs) include spin-transfer torques (STTs) in perpendicular magnetic tunnel junctions [1,7–12] and, more recently, spin-orbit torques (SOTs) in symmetry-broken ferromagnet and non-magnet (NM) bilayers [13–15]. In typical NM and FM heterostructures, such as in W-, Pt-, or Ta-based bilayers, the conventional spin Hall effect in the bulk of the NM provides an efficient mechanism to generate and inject spin currents, characterized by orthogonal spin and flow directions, into the adjacent FM. We call the ensuing torques "conventional spin-orbit torque" (CSOT). For bilayers

comprising NMs with a broken mirror plane symmetry, unconventional symmetry-allowed spin currents displaying a spin-polarization axis aligned with the flow direction are produced [13–16]. The injection of such spin currents into an adjacent FM imparts a spin torque, which we call "unconventional spin-orbit torque" (USOT). Magnetization control through the simultaneous impact of CSOT and USOT holds promise to enable deterministic and highly energy-efficient field-free switching of PMA FMs beyond what is currently possible with regular STT or CSOT alone.

We note that other improvements over CSOT-based switching have been proposed [17–21]; a recent study indicated that the presence of dampinglike torques generated by symmetry breaking in a trilayer geometry can dramatically reduce the critical current density and induced deterministic switching of a PMA FM [17]. The enhancement in efficiency relies on the fact that such symmetry-breaking dampinglike torque directly competes with the intrinsic damping of the PMA FM, overcoming the damping-independent critical current density associated

_____

*sousa020@umn.edu
†tlow@umn.edu

with dampinglike CSOT switching. Hybrid STT-assisted CSOT schemes were also shown to enable efficient and deterministic switching of a PMA FM [18–21]. Here, the free PMA FM is simultaneously subjected to CSOTs, from conventional spin Hall current originating in the bulk of the NM, and symmetry-breaking STTs, from the injection of out-of-plane spin-polarized currents due to the presence of a fixed PMA FM layer. A common feature of these approaches is the presence of additional ferromagnetic elements to induce symmetry breaking and allow deterministic switching of the PMA FM. In this sense, CSOT-USOT-based devices have the advantage of requiring simpler architecture with separated write and read current paths, as it does not rely on the presence of more complicated arrangements. Additionally, it is potentially more energy efficient due to the considerable amount of promising symmetry-broken NMs, some of which are predicted to display giant unconventional spin Hall effects [22].

Theoretical and experimental developments have shown that fieldlike SOTs can directly impact the dynamical state of a magnetization in a bilayer geometry [23–27]. For instance, fieldlike CSOTs have been shown to greatly influence the threshold switching condition by introducing a half-integer power dependence of the damping constant to the critical switching current [23]. Recent experiments revealed the existence of large fieldlike CSOTs in Ru_2Sn_3/Co-Fe-B bilayers [24], which was also shown to substantially modify the dynamical state of the in-plane FM layer. From these developments, one might anticipate that fieldlike CSOTs might also play a role in determining the dynamical states of a PMA FM simultaneously subjected to CSOT and USOTs. Hence, the evaluation of the field-free switching state diagram of a PMA FM, including the impact of fieldlike CSOTs and USOTs, becomes crucial in accessing the potential of such symmetry-broken bilayers for highly energy-efficient switching applications, which has not yet been investigated in detail.

In this work, we numerically compute field-free state diagrams for a perpendicular magnetization simultaneously subjected to fieldlike and dampinglike CSOT and USOT. Our analysis reveals unanticipated dynamical regimes characterized by stable precessional and pinned states whose existences are strongly connected to the sign and strength of the fieldlike CSOT. We find that energy-efficient field-free switching might not be achieved by simultaneously maximizing the spin Hall angles associated with CSOTs and USOTs. Instead, while large spin Hall angles associated with USOT are always beneficial, there is an ideal CSOT spin Hall angle for which highly energy-efficient switching takes place. Our work offers a systematic pathway to realizing energy-efficient switching of a perpendicular magnetization in symmetry-broken bilayer heterostructures.

II. THEORETICAL MODEL

We study a bilayer heterostructure comprised of a thin PMA FM overlaid on a strongly spin-orbit-coupled symmetry-broken NM. The reduced symmetry is assumed to be an intrinsic property of the crystal structure of the NM. The relevance of such a feature is illustrated in Figs. 1(a) and 1(b), where we compare the spin Hall response of two fictitious NMs with distinct degrees of symmetry; for the NM slab with two mirror planes, M_{xz} and M_{yz} [shown in Fig. 1(a)], only M_{xz} remains a symmetry of the system under an applied electric field along the x direction. In this scenario, the presence of M_{xz} constrains the spin Hall response to produce spin currents with mutually orthogonal spin and flow directions (black flowing spins). On the other hand, the symmetry-broken NM slab with a single mirror plane, M_{yz} [shown in Fig. 1(b)], is left without any mirror symmetry under the action of
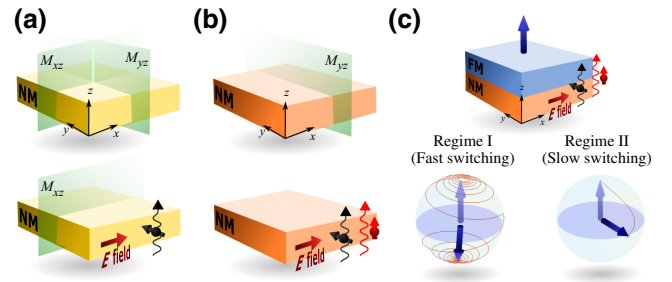

FIG. 1. Spin Hall responses of fictitious nonmagnetic (NM) slabs with varying degrees of crystalline symmetries, as exemplified by the number of mirror planes, and sample magnetization trajectories of a perpendicular ferromagnet subjected to the derived spin-orbit torques. (a) NM slab with two mirror planes M_{xz} and M_{yz}; because the mirror plane M_{xz} is still a symmetry of the NM slab when the electric field is applied along the x direction, the spin Hall response is constrained by the remaining symmetry to produce spin currents whose flow and spin directions are mutually orthogonal to each other and to the electric field (bottom figure). (b) NM slab with single mirror plane M_{yz}; because the electric field along the x direction breaks the only mirror plane available, the spin Hall response gives rise to conventional (black flowing spins) as well as unconventional (red flowing spins) spin currents, where the later is characterized by collinear spin and flow directions that are orthogonal to the electric field (bottom figure). (c) Bilayer heterostructure comprised of a ferromagnet (top layer) and a strong spin-orbit-coupled NM layer with a single-crystal yz mirror plane. An electric field applied along the x direction generates SOTs on the perpendicular magnetization due to conventional and unconventional spin Hall effects. The interplay between CSOT and USOT leads to the existence of distinctive dynamical regimes. The bottom figures illustrate dynamical regimes where full switching and full in-plane damping of the magnetization are expected. We note that switching to the $-\hat{z}$ direction in regime I is faster than switching in regime II in the small intrinsic damping limit.

an electric field applied along the x direction. Consequently, the spin Hall response is not constrained, which enables unconventional spin Hall currents with collinear spin and flow directions (red flowing spins) in addition to the conventional response.

A symmetry-broken bilayer heterostructure composed of a PMA FM and the NM with a single mirror plane is illustrated in Fig. 1(c). Here, an in-plane electric field generates a SOT on the magnetization of the FM due to a flow of spin-polarized electrons originating from the spin Hall effect in the bulk of the NM. Assuming an electric field applied along the x direction, the generated spin currents in the bulk of the NM are $Q_z^y = \sigma_{zx}^y E_x$ and $Q_z^z = \sigma_{zx}^z E_x$, where the subscripts refer to the flow direction and the superscripts to the spin-quantization axis, as sketched in Fig. 1(c). The former component, associated with σ_{zx}^y, is the conventional spin Hall response, where field, spin, and flow directions are mutually orthogonal to each other. The latter component, associated with σ_{zx}^z, is the unconventional response that exists only due to the lack of a xz mirror plane in the NM. The transfer of spin angular momentum from the spin Hall currents to the magnetization imparts a total SOT, which can be classified as damping- and fieldlike CSOT and USOT. A promising example of such a system is that of $1T' - \text{WTe}_2/\text{Py}$ bilayers, whose USOT was recently observed in experiments [13,15,28]. Symmetry-dependent USOT-based switching was also observed in CuPt/CoPt bilayers [29], which is equally well described by the model presented here in spite of the richer lattice symmetries of $L1_1$-ordered Cu(Co)Pt crystals. In our study, the perpendicular anisotropy axis of the FM layer coincides with the z axis.

The total SOT torque density is

$$\mathcal{N} = \tau_{DL}^y \hat{\mathbf{m}} \times (\hat{\mathbf{m}} \times \hat{\mathbf{y}}) + \tau_{FL}^y \hat{\mathbf{m}} \times \hat{\mathbf{y}} + \tau_{DL}^z \hat{\mathbf{m}} \times (\hat{\mathbf{m}} \times \hat{\mathbf{z}}) + \tau_{FL}^z \hat{\mathbf{m}} \times \hat{\mathbf{z}}, \quad (1)$$

where $\tau_{DL}^{y(z)} = (\hbar/2e)\theta_{y(z)}J$ and $\tau_{FL}^{y(z)} = \beta\tau_{DL}^{y(z)}$ are the dampinglike and fieldlike contributions, respectively, with J being the applied current density. For simplicity we assume that β is the same for both y and z spin components. The conventional (unconventional) spin Hall angle is defined as $\theta_{y(z)} = (2e/\hbar)\sigma_{zx}^{y(z)}/\sigma_{xx}$. The damping- and fieldlike CSOT and USOT are depicted over the unit sphere in Fig. 2; the red arrows represent the specific normalized SOT acting on the magnetization whose direction is defined by a single point on the surface of the sphere. While the dampinglike CSOT (USOT) relaxes the magnetization towards the $-\hat{\mathbf{y}}$ ($-\hat{\mathbf{z}}$) direction, the associated fieldlike torque causes the magnetization to undergo precession around the $\hat{\mathbf{y}}$ ($\hat{\mathbf{z}}$) direction.
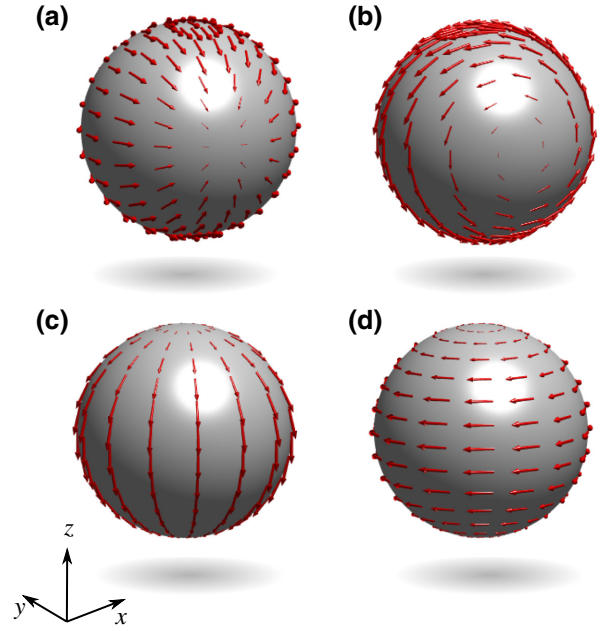

FIG. 2. Depiction of the spin-orbit fieldlike and dampinglike torques over the unit sphere. The conventional dampinglike and fieldlike torques are shown in (a),(b), respectively. The unconventional dampinglike and fieldlike spin-orbit torques are depicted in (c),(d), respectively. These correspond to the four terms in the spin-orbit torque density in the Landau-Lifshitz-Gilbert equation, as defined in Eq. (1).

The Landau-Lifshitz-Gilbert (LLG) equation governing the magnetization dynamics reads

$$\frac{d\hat{\mathbf{m}}}{dt} = -\gamma\hat{\mathbf{m}} \times \mathbf{H}_{\text{eff}} + \alpha\hat{\mathbf{m}} \times \frac{d\hat{\mathbf{m}}}{dt} + \frac{\gamma}{\mu_0 M_S d}\mathcal{N}, \quad (2)$$

where $\hat{\mathbf{m}} = \mathbf{M}/M_S$ with $\mathbf{M}$ being the magnetization of the FM film with saturation value M_S, γ is the gyromagnetic ratio, α is the intrinsic damping parameter, μ_0 is the vacuum permeability and d is the thickness of the ferromagnetic film. The perpendicular magnetic anisotropy is described through the effective field $\mathbf{H}_{\text{eff}} = (2K_{\text{eff}}/\mu_0 M_S)(\hat{\mathbf{m}} \cdot \hat{\mathbf{z}})\hat{\mathbf{z}}$ with $\hat{\mathbf{z}}$ being perpendicular to the interface plane. The effective anisotropy parameter K_{eff} is related the interfacial anisotropy constant K_i as $K_{\text{eff}} = K_i/d - \mu_0 M_S^2/2$. In the following, we numerically solve Eq. (2) for the time evolution of $\hat{\mathbf{m}}$ and explore the simultaneous impact of θ_y and θ_z on the magnetization dynamics.

III. PRELIMINARY DISCUSSION

In general, the qualitative aspects of the magnetization dynamics expected for such a system depends upon the relative magnitude of the various parameters involved. We start by distinguishing two of the main dynamical regimes, which will be referred to as regimes I and II [in the bottom

panel of Fig. 1(c)]. In regime I, the dynamics is characterized by a switching event similar to that induced by spin-transfer torque in perpendicular magnetic tunnel junctions [10], i.e., the magnetization relaxes to a stable focus at $\hat{\mathbf{m}} \approx -\hat{\mathbf{z}}$ as shown in Fig. 1(c). Here, the dampinglike torque attributed to θ_z dominates the dynamics by overcoming the intrinsic damping of the FM layer, whereas the overall effect of θ_y is to modify the precessional rates during the dynamical evolution and to cause a small tilt of the final magnetization configuration away from $-\hat{\mathbf{z}}$. The latter feature and intrinsic damping ensures deterministic switching to the $\hat{\mathbf{m}} = -\hat{\mathbf{z}}$ configuration when the applied current pulse vanishes.

In regime II, the dynamics is characterized by a steady state where the magnetization is damped towards $\hat{\mathbf{m}} \approx -\hat{\mathbf{y}}$, as shown in Fig. 1(d). In this regime, the dampinglike torque attributed to θ_y dominates the dynamics, whereas the θ_z causes only a small tilt of the final magnetization configuration towards the $-\hat{\mathbf{z}}$ direction. Here, deterministic switching to the $\hat{\mathbf{m}} = -\hat{\mathbf{z}}$ configuration might not occur when the applied current passing through the NM is turned off, particularly if thermal fluctuations are strong enough. Hence, while regime I supports deterministic switching of the perpendicular magnetization, regime II does not necessarily. If thermal fluctuations are weak, regime II may also lead to switching after the current pulse has vanished. Here, the intrinsic damping of the FM layer guarantees that the perpendicular magnetization relaxes from approximately equal to $-\hat{\mathbf{y}}$ towards $-\hat{\mathbf{z}}$ if there exists a small downward tilting due to θ_z. However, this process is very slow due to the smallness of intrinsic damping parameters in typical transition metal-based FM layers. Therefore, switching in regime I is much faster than switching in regime II in the small damping limit.

The distinction between regimes I and II provides a starting point for understanding the system behavior, however we see that the full spectrum of system behavior includes several other regimes, such as precessional and pinned states. One key factor determining the system behavior is the relative orientation between the magnetization and the spin direction of the incoming spin current. For incoming spin oriented perpendicular to the magnetization, the dampinglike torque competes directly with the torque from anisotropy. On the other hand, for nearly collinear magnetization and incoming spin, the dampinglike torque competes with the torque from magnetic damping, which is weaker by a factor of α. Accordingly, the critical current for switching is a factor α smaller for collinear incoming spin and magnetization, compared to perpendicular incoming spin and magnetization.

We find that the fieldlike CSOT plays a key role in the dynamics. This is due to the fact that the fieldlike CSOT tilts the magnetization away from the anisotropy axis towards the y axis by a small amount θ_{tilt} (see Fig. 3). The direction of the tilt depends on the sign of β. Figure 3
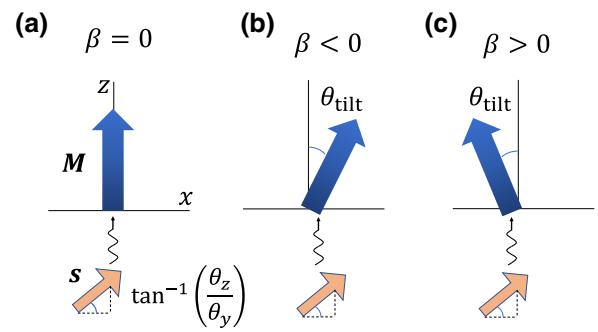

FIG. 3. Schematic of the key factors controlling the magnetic dynamics. The magnetization (blue arrow) has an effective easy axis, which is determined by the magnetic anisotropy and the fieldlike torque, which tilts the magnetization from the z axis by an amount θ_{tilt}. The incoming spin direction (orange arrow) is determined by θ_z/θ_y. The squiggly arrow denotes velocity direction of spin current. The critical switching current is decreased when the magnetization and incoming spin are more aligned, as in (b).

shows different scenarios. If the magnetization is tilted toward (away) from the incoming spin, the critical current decreases (increases), due to the factors described in the previous paragraph. For this reason, we find that the fieldlike torque plays a role in determining the magnetic dynamics.

IV. CURRENT-INDUCED DYNAMICAL STATE TRANSITIONS

In this section we show that a current-induced transition between regimes I and II takes place and is highly affected by the strength and sign of the fieldlike to dampinglike torque ratio as quantified by β [30]. We focus on describing magnetization dynamics of PMA FMs with small intrinsic damping, $\alpha = 0.001$. We assume the following parameters throughout: $d = 1$ nm, $K_{\text{eff}} = 2 \times 10^5$ J/m^3, and $M_S = 1.27 \times 10^6$ A/m.

First, we study the current-induced transition at *negative* β; we take $\beta = -0.2$. Figure 4 displays the time evolution of the magnetization components due to CSOT and USOT quantified by the spin Hall angles $\theta_y = 0.6$ and $\theta_z = 0.05$, respectively, at two current densities. At lower currents ($J = 0.60 \times 10^7$ A/cm^2), magnetization reversal takes place with $\hat{\mathbf{m}}(t = +\infty) \approx -\hat{\mathbf{z}}$, with initial condition $\hat{\mathbf{m}}(t = 0) \approx \hat{\mathbf{z}}$. This situation is shown in Fig. 4(a) and characterizes a magnetization dynamics of regime I. Upon increasing the applied current density, the switched steady state slowly deviates from the $\approx -\hat{\mathbf{z}}$ until an abrupt transition to an alternative in-plane steady state with $\hat{\mathbf{m}}(t = +\infty) \approx -\hat{\mathbf{y}}$ takes place at a critical current density. The time evolution of the magnetization components for a slightly larger current density of $J = 0.61 \times 10^7$ A/cm^2 (the critical current) is shown in Fig. 4(b). Therefore, we
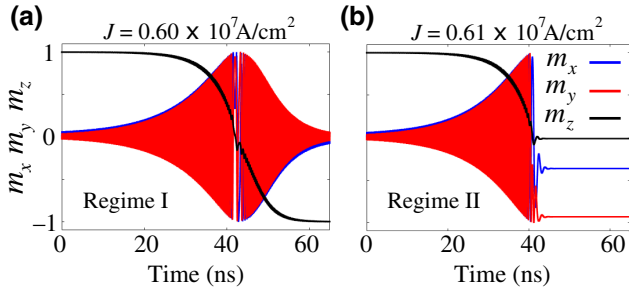
FIG. 4. Time evolution of the components of the magnetization at a *negative* fieldlike to dampinglike torque ratio of $\beta = -0.2$. Upon increasing the applied current density from (a) $J = 0.60 \times 10^7$ A/cm^2 to (b) $J = 0.61 \times 10^7$ A/cm^2, with $\theta_y = 0.6$ and $\theta_z = 0.05$, a transition from dynamical regime I to regime II takes place.

conclude that a *direct* transition between regimes I and II can be induced by current in the negative β case. The evolution of the transition point with the strength of β will be addressed in upcoming sections.

We now focus on the current-induced dynamical regime transition considering *positive* fieldlike to dampinglike torque ratios. For the sake of comparison, all parameters are assumed to be the same as the previous calculation except for the sign of β, i.e., $\beta = +0.2$. Figure 5 shows the time evolution of the magnetization due to CSOT and USOT at increasing current densities. We observe in Fig. 5(a) that the dynamics excited by a current density of $J = 1.2 \times 10^7$ A/cm^2 falls within regime I. This is in sharp contrast to the $\beta < 0$ case, where the dynamics induced by the same current density resides in regime II.

An *indirect* current-induced transition to regime II that takes place at $\beta > 0$, in contrast with the $\beta < 0$ scenario. Here, a larger current density induces transitions to intermediate dynamical regimes before the full transition to regime II. This is shown in Figs. 5(b) and 5(c), where transitions to a stable precessional and steady states occur upon increasing the current density to $J = 1.3 \times 10^7$ A/cm^2 and subsequently to $J = 8.0 \times 10^7$ A/cm^2, respectively. Transition to regime II occurs at much larger current densities, as shown in Fig. 5(d) for $J = 9.0 \times 10^7$ A/cm^2. The inset shows in detail the typically damped time evolution of the magnetization components in the $\beta > 0$ [23], which is qualitatively distinct from the regime II oscillatory behavior for the $\beta < 0$ in Fig. 4(b).

The above discussion indicates that the sign of β is crucial in determining the condition for full reversal of a perpendicular magnetization simultaneously subjected to CSOT and USOT. The observation that larger current densities might actually be detrimental to an already switched configuration by inducing transitions to a precessional state shows that a full state diagram covering the various dynamical regimes over a given parameter space is necessary for further guiding experimental work in this
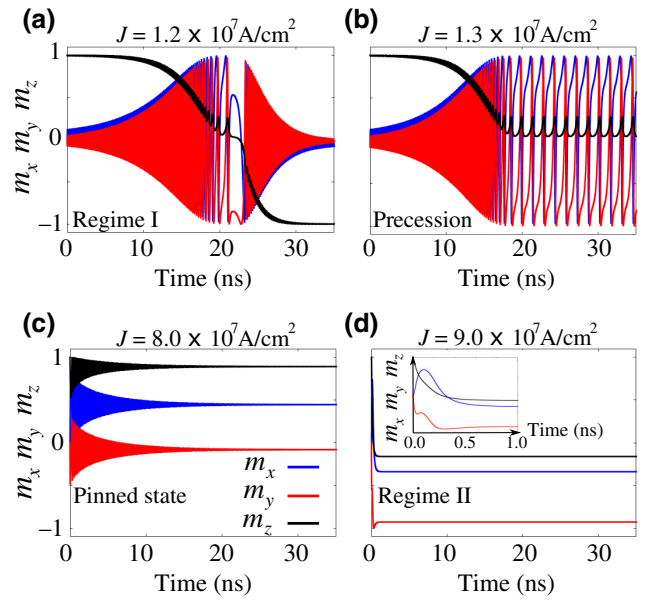

FIG. 5. Time evolution of the components of the magnetization at a *positive* fieldlike to dampinglike torque ratio of $\beta = +0.2$. Here, transitions between dynamical regimes I and II take place through intermediate stable precessional and pinned state regimes: (a) $J = 1.2 \times 10^7$ A/cm^2 (b) $J = 1.3 \times 10^7$ A/cm^2, (c) $J = 8.0 \times 10^7$ A/cm^2, and (d) $J = 9.0 \times 10^7$ A/cm^2, with $\theta_y = 0.6$ and $\theta_z = 0.05$.

field. In the following, we construct and discuss the main characteristics of relevant state diagrams.

V. DYNAMICAL STATE DIAGRAMS

We provide insights into the various dynamical regimes of a perpendicular magnetization subjected to CSOT and USOT by constructing two main state diagrams: a current density versus β at fixed conventional and unconventional spin Hall angles ($\theta_y = 0.6$ and $\theta_z = 0.05$) and a θ_y versus θ_z state diagram at fixed $J = 3.0 \times 10^7$ A/cm^2 and $\beta = +0.2$. The diagrams are constructed by numerically obtaining the boundaries between distinct dynamical regimes over the given parameter space. The boundaries are easily identified through sharp changes in magnetization dynamics at critical parameter values, as shown in (a) and (b) in Figs. 4 and 5.

The state diagrams are presented in Fig. 6, where distinct dynamical regimes are highlighted by different colors. The symbols demarcating the boundaries are the numerically obtained critical transition points. The J versus β state diagram in Fig. 6(a) reveals a single transition boundary between regimes I and II at all negative β cases we consider. Here, the critical current density necessary to induce a dynamical state transition to regime II decreases with increasing $|\beta|$, consistent with previous predictions [23]. At $\beta > 0$, there also exists a single transition boundary between regimes I and II for $\beta < 0.145$, but with
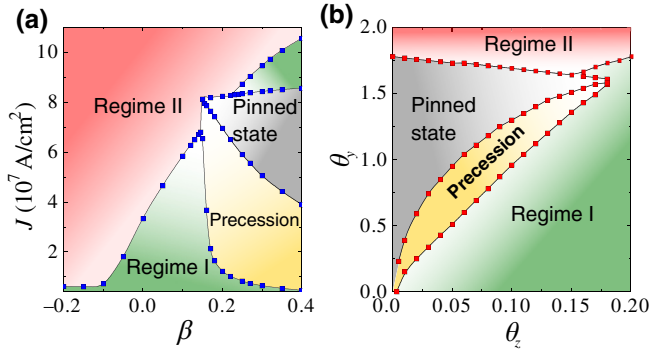
FIG. 6. Switching diagrams of a perpendicular magnetization subjected to both CSOT and USOT. (a) Current density × field-like to dampinglike torque ratio switching diagram at fixed $\theta_y = 0.6$ and $\theta_z = 0.05$. (b) θ_y versus θ_z switching diagram at fixed $J = 3 \times 10^7$ A/cm^2 and $\beta = +0.2$. Distinct dynamical regimes are represented by different colors. The boundary lines are obtained numerically by inspecting the full magnetization dynamics using the LLG equation.

the critical current density being an increasing function of $|\beta|$. Beyond the critical value $\beta \approx 0.145$ there appears intermediate dynamical regimes characterized by stable precessional and steady states. Hence, we conclude that there exists a critical $\beta > 0$ separating direct and indirect transitions between regimes I and II, beyond which our results indicate an expansion (contraction) of the steady state (precessional state) region with further increase β. We note that the large current-density window within which the precessional states exist at a given $\beta > 0.145$ might be ideal for applications in nano-oscillators that are robust to current-density variations. We stress that further studies are necessary to address the potential of the precessional states for applications, which is beyond the scope of this work.

In Fig. 6(b) we show the spin Hall angle state diagram at fixed $J = 3 \times 10^7$ A/cm^2 and $\beta = 0.2$. Here, the β value is chosen to enable the analysis of the evolution of all distinct dynamical regimes with θ_y and θ_z. The state diagram shows that while the extent of regime II is limited to large θ_y values ($\theta_y > 1.5$), regime-I-type dynamics is possible for unconventional spin Hall angles as small as $\theta_z \approx 0.01$ at sufficiently small θ_y. Notice that regime I is only accessible at finite θ_z. Our numerical results indicate that spin Hall angle ratios of $\theta_z/\theta_y \approx 10\%$ are enough to induce a regime-I-type dynamics, i.e., full magnetization reversal of a perpendicular magnetization. The possibility of full magnetization switching at small θ_z/θ_y ratios is tightly connected to the fact that, while CSOT are required to overcome the anistropy field for full switching, the dampinglike USOT has to counteract the much smaller intrinsic damping. In this sense, the USOT is promoted to the role of being the main switching agent, whereas the conventional one provides an assisting mechanism.

The above picture is supported by experimentally observed magnetization switching in $1T' - WTe_2/Py$ bilayers where $\theta_z/\theta_y \approx 24\%$ [28]. Other symmetry-broken NMs potentially suitable for observing the effects mentioned above are $BiTe_3$, $Ni_2P_6W_4$, and $Ba_2C_4S_4N_4$, to cite a few, all of which display giant σ_{zx}^z above 1000 $(\hbar/2e)\Omega^{-1}$ cm^{-1} [22].

Figure 6(b) also indicates an unanticipated scenario in which large conventional spin Hall angles become detrimental to deterministic switching of a perpendicular magnetization; upon further increasing θ_y beyond the critical boundary line at fixed θ_z, full magnetization reversal is suppressed due to transitions to precessional and steady-state regimes. Hence, we obtain the unexpected result that larger conventional spin Hall angles might be detrimental to switching in symmetry-reduced bilayer heterostructures.

In the following section, we provide a qualitative description of the above behavior from an analytical toy-model perspective. Our analysis indicates that upon increasing θ_y, an effective easy-axis tilting induced by the fieldlike CSOT develops, altering the switching threshold condition. The tilt depends on the sign of β, providing an explanation for the disparate behavior shown in Fig. 6(a) for $\beta > 0$ and $\beta < 0$.

VI. IMPACT OF FIELDLIKE TORQUES: A MODEL DESCRIPTION

We next present an analytical model to describe some of the qualitative features of the numerical data presented in the previous section. We begin by noting that the tilt of the magnetization is given by

$$\tan \theta_{\text{tilt}} = \beta \frac{\hbar}{4e} \theta_y \frac{J}{K_{\text{eff}} d}. \quad (3)$$

We assume that the only effect of the fieldlike torque is to tilt the uniaxial anisotropy axis by a small amount of θ_{tilt} [31]. Within this approximation, the critical switching current due to CSOT and USOT is obtained by rotating the coordinate system by θ_{tilt} so as to align the alternative z axis with the tilted main anisotropy axis. The net effect on the spin quantization axis of the incoming spin current amounts to taking the effective spin Hall angles $\tilde{\theta}_z$ and $\tilde{\theta}_y$ according

$$\begin{pmatrix} \tilde{\theta}_z \\ \tilde{\theta}_y \end{pmatrix} = \begin{pmatrix} \cos \theta_{\text{tilt}} & -\sin \theta_{\text{tilt}} \\ \sin \theta_{\text{tilt}} & \cos \theta_{\text{tilt}} \end{pmatrix} \begin{pmatrix} \theta_z \\ \theta_y \end{pmatrix}, \quad (4)$$

where the sign of θ_{tilt} is determined by the sign of the field-like to dampinglike torque ratio β. Hence, for $\beta < 0$ we take $\theta_{\text{tilt}} \to -\theta_{\text{tilt}}$ in Eq. (4).

The critical switching current in the rotated coordinate systems is approximately given by [17]

$$J_{\text{sw}}(\theta_{\text{tilt}}) = \frac{4eK_{\text{eff}}d}{9\alpha\hbar} A(\theta_{\text{tilt}}) B(\theta_{\text{tilt}}) \frac{\tilde{\theta}_z}{\tilde{\theta}_y^2}, \quad (5)$$

where we define

$$A(\theta_{\text{tilt}}) = -1 + \sqrt{1 + 6\alpha^2 \left(\frac{\tilde{\theta}_y}{\tilde{\theta}_z} \right)^2}, \qquad (6a)$$

$$B(\theta_{\text{tilt}}) = \sqrt{3 + \frac{12}{2 + A(\theta_{\text{tilt}})}}. \qquad (6b)$$

The form for the critical current can be intuitively understood in some limiting cases that we describe next. These limiting cases provide a way to qualitatively understand the impact of fieldlike torques on the dynamical state of the perpendicular magnetization.

We first consider $\beta > 0$ and assume that the incoming spin is perpendicular to the tilted anisotropy axis. The effective spin Hall angles in the rotated coordinates' system become $\tilde{\theta}_y \to \theta_y / \cos(\theta_{\text{tilt}})$ and $\tilde{\theta}_z \to 0$. Hence, the excited magnetization dynamics in the rotated coordinates' system is dominated by a dampinglike torque due to incoming spin currents with polarization direction transverse to the main tilted anisotropy axis. This scenario is similar to that in bilayer heterostructures under the action of CSOTs, which exhibit critical switching currents that are independent of α [17,23,32]. Accordingly, we find the critical switching current is given by

$$J_{\text{sw}}^{\beta > 0} \approx \frac{4\sqrt{2}e}{3\hbar} \frac{K_{\text{eff}}d}{\theta_y}, \qquad (7)$$

which is larger than $J_{\text{sw}}(\theta_{\text{tilt}} = 0)$, in Eq. (5), by a factor of approximately equal to α^{-1}.

We next consider $\beta < 0$ and assume the incoming spin direction is collinear to the tilted anisotropy axis. The effective spin Hall angles in the rotated coordinates' system become $\tilde{\theta}_y \to 0$ and $\tilde{\theta}_z \to \theta_y / \cos(\theta_{\text{tilt}})$. Here, the magnetization dynamics is dominated by dampinglike torques due to incoming spin currents with polarization direction aligned with the main tilted anisotropy axis. In this situation, the dampinglike torque directly competes with intrinsic damping, resulting in critical switching current proportionals to α. Indeed, the critical switching current is

$$J_{\text{sw}}^{\beta < 0} \approx \frac{4e}{\hbar} \alpha \frac{K_{\text{eff}}d}{\theta_z}, \qquad (8)$$

which is smaller than $J_{\text{sw}}(\theta_{\text{tilt}} = 0)$ of Eq. (5) in the small damping limit.

The above discussion indicates that the sign and strength of the conventional fieldlike to dampinglike torque ratio is crucial in determining the current threshold condition for switching. This observation results in the following picture; the amount of anisotropy axis tilting due to the conventional fieldlike torque is determined by β as well as the applied current density J, as described in Eq. (3).

If $\beta > 0$ ($\beta < 0$), a new switching current threshold will be established by the induced tilting, θ_{tilt}. Hence, the applied current density J determines an alternative current switching threshold $J_{\text{sw}}^{\beta > 0(\beta < 0)}$ in accordance to the β.

As a consequence, the threshold condition to excite magnetization dynamics within regime I will depend on θ_z and θ_y, as well as on J and β. This implies that an initially stable regime-I-type dynamics induced by a current density J might not be made possible by further increasing the applied current density due to a larger switching threshold induced by the tilting. This is also possible for systems with larger θ_y [see Eq. (3)], leading to the conclusion that NM layers displaying large conventional spin Hall angles might prevent deterministic SOT switching in symmetry-broken bilayer heterostructures. Our analysis suggests that regime-I-type dynamics is prevented in the limit $\tan(\theta_{\text{tilt}}) \to \theta_z / \theta_y$ where

$$\frac{\theta_z}{\theta_y^2} = \frac{\hbar}{4e} \beta \frac{J}{K_{\text{eff}}d}, \qquad (9)$$

beyond which an alternative dynamical regime, other than regimes I and II, must exist. We emphasize that Eq. (9) does not offer a quantitative description of the regime-I boundary at larger θ_y values due to our initial assumptions of small θ_{tilt}. The generalization of Eq. (9) for arbitrary θ_y will be left for a future work. We note that this law described the $\beta > 0$ situation. As for the $\beta < 0$, the transition to regime II can be estimated by Eq. (22) of Ref. [23], which sets the limit θ_y for optimizing switching.

Therefore, we conclude that the fieldlike torque due to the CSOT is the main agent behind the existence of stable precessional and steady-state regimes. This observation is extremely useful in guiding the search of symmetry-broken spin Hall channels displaying both σ_{zx}^y and σ_{zx}^z for efficient switching of a perpendicular magnetization. Because fieldlike SOTs are always present in bilayer heterostructures, our results suggest that one should look into materials displaying large θ_z while maintaining θ_z / θ_y limited to the regime-I region of the state diagram in Fig. 6(b). This condition necessarily implies the existence of an optimal θ_y, contrary to the common belief of maximizing both θ_y and θ_z for efficient magnetization reversal. The deterministic switching optimization is discussed next.

VII. OPTIMIZING DETERMINISTIC SWITCHING

Our previous results have established that full deterministic switching takes place within the limited region of the parameter space corresponding to regime I. We now address the question of how deterministic switching can be further optimized within this dynamical regime. To tackle this problem, we study the parameter dependence of the normalized energy delay product, $E_{\text{sw}} \tau_{\text{sw}} \propto (J\tau_{\text{sw}})^2$, where E_{sw} and τ_{sw} are the switching energy and time associated

with a current density J. This figure of merit captures the application need for switching, which is both low energy and fast.

In the dynamical regime I, the switching time τ_{sw} is obtained numerically by registering the time spent for full magnetization reversal according to the criteria $m_z(\tau_{sw}) < -0.95$ and $(dm_z/dt)_{t=\tau_{sw}} < 0.01$, at every point of a given parameter space. The normalized energy-delay product in a J versus β state diagram, at fixed $\theta_y = 0.6$ and $\theta_z = 0.05$, is shown in Fig. 7(a), where the darker regions correspond to dynamical regimes other than regime I. The result shows that there exists an optimum switching efficiency at positive β, where the energy-delay product can be reduced by approximately 50% of its maximum value [see darker blue region in Fig. 7(a)]. Further, we notice that the associated optimum current density is higher than the regime-I threshold switching current. This is due to the fact that the rate of decay of the switching time with the applied current density is faster than the rate of increase of J at lower current density. However, the rate of decay of the switching time shows down near the regime-I boundaries, such that the
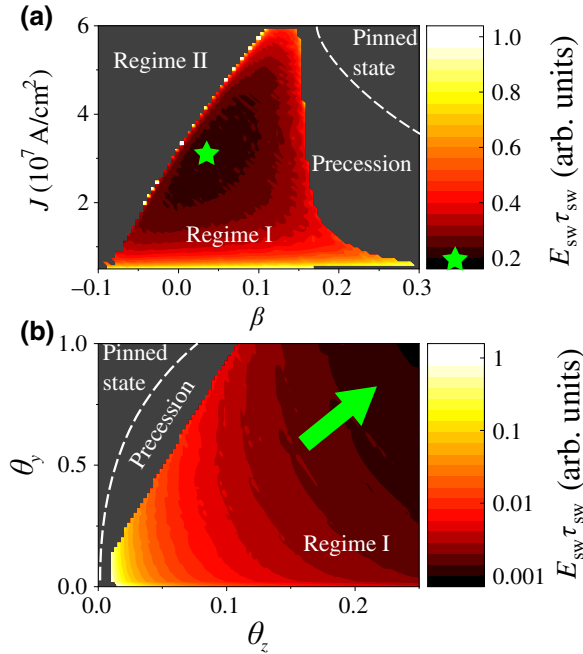
product $J\tau_{sw}$ becomes an increasing function of J. Therefore, an optimum current density exists and corresponds to a minimum of $J\tau_{sw}$.

Figure 7(b) displays the normalized energy-delay product in a θ_y versus θ_z state diagram at fixed $J = 3 \times 10^7$ A/cm^2 and $\beta = +0.2$. The efficiency is normalized to that corresponding to the minimum spin Hall angles necessary to attain full switching at the given J and β values: $\theta_y = 0$ and $\theta_z = 0.015$. Here, efficiency is a monotonic function of the unconventional spin Hall angle with the possibility of attaining several orders of magnitude improvement upon increasing θ_z. On the other hand, we also observe that virtually no efficiency improvement is attained at larger θ_y. Instead, larger θ_y might actually prevent deterministic switching by inducing transitions to precessional states, as previously discussed.

The above results establish that the largest source of efficiency improvement within regime I is the unconventional spin Hall angle. Although an optimized current density can be found, deterministic switching becomes much more efficient in bilayers composed of materials displaying larger θ_z values and an optimal ratio θ_z/θ_y. A few tentative bilayer structures composed of symmetry-broken NMs potentially suitable for observing the effects mentioned above are Co-Fe-B(Py)/BiTe$_3$, Co-Fe-B(Py)/Ni$_2$P$_6$W$_4$, Co-Fe-B(Py)/Ba$_2$C$_4$S$_4$N$_4$ [22] or Py/SrIrO$_3$. The latter was recently investigated experimentally in the context of CSOTs [33] with the prediction of giant unconventional spin Hall effects in orthorhombic SrIrO$_3$ [34].

VIII. CONCLUSIONS

We study the simultaneous impact of CSOT and USOT on the dynamics of a perpendicular magnetization in bilayer heterostructures in the small intrinsic damping limit. Our results reveal that the fieldlike CSOT immensely impacts the dynamical state of the perpendicular magnetization, leading to the formation of distinctive dynamical regimes over relevant parameter spaces. Particularly, we show the existence of unexpected stable precessional and steady states at larger conventional spin Hall angles. This implies that nonmagnets displaying large conventional spin Hall angles, θ_y, might be detrimental to full deterministic switching in this system. We also establish that highly efficient deterministic switching is attained at larger unconventional spin Hall angles, θ_z, within a specific dynamical regime constrained by the ratio θ_z/θ_y. Our work clarifies the physics and performance metric necessary for highly energy-efficient switching of a perpendicular magnetization in symmetry-broken bilayer heterostructures.

FIG. 7. Regime I normalized switching energy-delay product, $E_{sw}\tau_{sw}$, of a perpendicular magnetization subjected to both CSOT and USOT. (a) Current density versus fieldlike to dampinglike torque ratio (J versus β) diagram, at fixed $\theta_y = 0.6$ and $\theta_z = 0.05$. The energy-delay product is normalized by that of $J = 0.5 \times 10^7$ A/cm^2 and $\beta = 0.15$. The green star highlights the optimal energy-delay product. (b) θ_y versus θ_z diagram, at fixed $J = 3 \times 10^7$ A/cm^2 and $\beta = +0.2$, where we normalize the energy-delay product by that of the case where $\theta_y = 0$ and $\theta_z = 0.015$. The green arrow indicates the direction of best energy-delay product. The darker regions correspond to dynamical regimes other than regime I.

———————————

[1] H. Meng and J.-P. Wang, Spin transfer in nanomagnetic devices with perpendicular anisotropy, Appl. Phys. Lett. **88,** 172506 (2006).

[2] S. Mangin, D. Ravelosona, J. A. Katine, M. J. Carey, B. D. Terris, and E. E. Fullerton, Current-induced magnetization reversal in nanopillars with perpendicular anisotropy, Nat. Mater. **5,** 210 (2006).

[3] M. Gajek, J. J. Nowak, J. Z. Sun, P. L. Trouilloud, E. J. O'Sullivan, D. W. Abraham, M. C. Gaidis, G. Hu, S. Brown, and Y. Zhu, *et al.*, Spin torque switching of 20 nm magnetic tunnel junctions with perpendicular anisotropy, Appl. Phys. Lett. **100,** 132408 (2012).

[4] D. Zhang, M. Bapna, W. Jiang, D. Sousa, Y.-C. Liao, Z. Zhao, Y. Lv, P. Sahu, D. Lyu, A. Naeemi, Tony Low, S. A. Majetich, and J.-P. Wang, Bipolar electric-field switching of perpendicular magnetic tunnel junctions through voltage-controlled exchange coupling, Nano Lett. **22,** 622 (2022).

[5] A. Sebastian, M. L. Gallo, R. Khaddam-Aljameh, and E. Eleftheriou, Memory devices and applications for in-memory computing, Nat. Nanotechnol. **15,** 529 (2020).

[6] W. Zhang, B. Gao, J. Tang, P. Yao, S. Yu, M.-F. Chang, H.-J. Yoo, H. Qian, and H. Wu, Neuro-inspired computing chips, Nat. Electron. **3,** 371 (2020).

[7] H. Suto, T. Nagasawa, T. Kanao, K. Yamada, and K. Mizushima, Magnetization switching of a perpendicular nanomagnet induced by vertical nonlocal injection of pure spin current, Sci. Rep. **9,** 19543 (2019).

[8] D. J. P. de Sousa, P. M. Haney, D. L. Zhang, J. P. Wang, and Tony Low, Bidirectional switching assisted by inter-layer exchange coupling in asymmetric magnetic tunnel junctions, Phys. Rev. B **101,** 081404(R) (2020).

[9] M. Lavanant, S. P.-Watelot, A. D. Kent, and S. Mangin, State diagram of a perpendicular magnetic tunnel junction driven by spin transfer torque: A power dissipation approach, J. Magn. Magn. Mater. **428,** 293 (2017).

[10] H. Liu, D. Bedau, J. Z. Sun, S. Mangin, E. E. Fullerton, J. A. Katine, and A. D. Kent, Dynamics of spin torque switching in all-perpendicular spin valve nanopillars, J. Magn. Magn. Mater. **358,** 233 (2014).

[11] S. Le Gall, J. Cucchiara, M. Gottwald, C. Berthelot, C.-H. Lambert, Y. Henry, J. Z. Sun, W. Lin, D. Ravelosona, J. A. Katine, Eric E. Fullerton, and S. Mangin, State diagram of nanopillar spin valves with perpendicular magnetic anisotropy, Phys. Rev. B **86,** 014419 (2012).

[12] W. H. Butler, T. Mewes, C. K. A. Mewes, P. B. Visscher, W. H. Rippard, S. E. Russek, and R. Heindl, Switching distributions for perpendicular spin-torque devices within the macrospin approximation, IEEE Trans. Magn. **48,** 4684 (2012).

[13] D. MacNeill, G. M. Stiehl, M. H. D. Guimaraes, R. A. Buhrman, J. Park, and D. C. Ralph, Control of spin-orbit torques through crystal symmetry in WTe$_2$/ferromagnet bilayers, Nat. Phys. **13,** 300 (2017).

[14] Fei Xue, C. Rohmann, J. Li, V. Amin, and P. M. Haney, Unconventional spin-orbit torque in transition metal dichalcogenide-ferromagnet bilayers from first-principles calculations, Phys. Rev. B **102,** 014401 (2020).

[15] Q. Xie, W. Lin, S. Sarkar, X. Shu, S. Chen, L. Liu, T. Zhao, C. Zhou, H. Wang, J. Zhou, S. Gradečak, and J. Chen, Field-free magnetization switching induced by the unconventional spin-orbit torque from WTe$_2$, APL Mater. **9,** 051114 (2021).

[16] M. Seemann, D. Ködderitzsch, S. Wimmer, and H. Ebert, Symmetry-imposed shape of linear response tensors, Phys. Rev. B **92,** 155138 (2015).

[17] D.-K. Lee and K.-Jin Lee, Spin-orbit torque switching of perpendicular magnetization in ferromagnetic trilayers, Sci. Rep. **10,** 1772 (2020).

[18] M. Wang, W. Cai, D. Zhu, Z. Wang, J. Kan, Z. Zhao, K. Cao, Z. Wang, Y. Zhang, T. Zhang, C. Park, J.-P. Wang, A. Fert, and W. Zhao, Field-free switching of a perpendicular magnetic tunnel junction through the interplay of spin-orbit and spin-transfer torques, Nat. Electron. **1,** 582 (2018).

[19] N. Sato, F. Xue, R. M. White, C. Bi, and S. X. Wang, Two-terminal spin-orbit torque magnetoresistive random access memory, Nat. Electron. **1,** 508 (2018).

[20] W. Cai, K. Shi, Y. Zhuo, D. Zhu, Y. Huang, J. Yin, K. Cao, Z. Wang, Z. Guo, Z. Wang, G. Wang, and W. Zhao, Sub-ns field-free switching in perpendicular magnetic tunnel junctions by the interplay of spin transfer and orbit torques, IEEE Electron Device Lett. **42,** 704 (2021).

[21] D. H. Kang and M. Shin, Critical switching current density of magnetic tunnel junction with shape perpendicular magnetic anisotropy through the combination of spin-transfer and spin-orbit torques, Sci. Rep. **11,** 22842 (2021).

[22] Y. Zhang, Q. Xu, K. Koepernik, R. Rezaev, O. Janson, J. Železný, T. Jungwirth, C. Felser, J. van den Brink, and Y. Sun, Different types of spin currents in the comprehensive materials database of nonmagnetic spin Hall effect, npj Comput. Mater. **7,** 167 (2021).

[23] T. Taniguchi, S. Mitani, and M. Hayashi, Critical current destabilizing perpendicular magnetization by the spin Hall effect, Phys. Rev. B **92,** 024428 (2015).

[24] T. J. Peterson, M. DC, Y. Fan, J. Chen, D. Zhang, H. Li, P. Swatek, J. G.-Barriocanal, and J.-P. Wang, Large fieldlike torque in amorphous Ru$_2$Sn$_3$ originated from the intrinsic spin Hall effect, Phys. Rev. Mater. **5,** 045003 (2021).

[25] M. Jiang, H. Asahara, S. Sato, S. Ohya, and M. Tanaka, Suppression of the field-like torque for efficient magnetization switching in a spin-orbit ferromagnet, Nat. Electron. **3,** 751 (2020).

[26] C. O. Avci, K. Garello, C. Nistor, S. Godey, B. Ballesteros, A. Mugarza, A. Barla, M. Valvidares, E. Pellegrin, A. Ghosh, I. M. Miron, O. Boulle, S. Auffret, G. Gaudin, and P. Gambardella, Fieldlike and antidamping spin-orbit torques in as-grown and annealed Ta/CoFeB/MgO layers, Phys. Rev. B **89,** 214419 (2014).

[27] J. Yoon, S.-W. Lee, J. H. Kwon, J. M. Lee, J. Son, X. Qiu, K.-J. Lee, and H. Yang, Anomalous spin-orbit torque switching due to field-like torque-assisted domain wall reflection, Sci. Adv. **3,** e1603099 (2017).

[28] S. Shi, J. Li, C.-H. Hsu, K. Lee, Y. Wang, L. Yang, J. Wang, Q. Wang, H. Wu, W. Zhang, G. Eda, G. Liang, H. Chang, and H. Yang, Observation of the out-of-plane polarized spin current from CVD grown WTe_2, Adv. Quantum Technol. **4,** 2100038 (2021).

[29] L. Liu, C. Zhou, X. Shu, C. Li, T. Zhao, W. Lin, J. Deng, Q. Xie, S. Chen, J. Zhou, R. Guo, H. Wang, J. Yu, S. Shi, P. Yang, S. Pennycook, A. Manchon, and J. Chen, Symmetry-dependent field-free switching of perpendicular magnetization, Nat. Nanotechnol. **16,** 277 (2021).

[30] We emphasize that the sign convention for β is tightly connected to the cross-product orderings of Eq. (1), which have not been consistent among different authors [17,23].

[31] This simplification is enabled by the fact that at sufficiently small θ_{tilt}, the overall damping profile over the unit sphere due to SOT and USOT is approximately the same as that of the case where $\theta_{tilt} = 0$ up to a small rotation of the coordinate system around the x axis.

[32] K.-S. Lee, S.-W. Lee, B.-C. Min, and K.-J. Lee, Threshold current for switching of a perpendicular magnetic layer induced by spin Hall effect, Appl. Phys. Lett. **102,** 112410 (2013).

[33] T. Nan, T. J. Anderson, J. Gibbons, K. Hwang, N. Campbell, H. Zhou, Y. Q. Dong, G. Y. Kim, D. F. Shao, T. R. Paudel, N. Reynolds, X. J. Wang, N. X. Sun, E. Y. Tsymbal, S. Y. Choi, M. S. Rzchowski, Y. B. Kim, D. C. Ralph, and C. B. Eom, Anisotropic spin-orbit torque generation in epitaxial $SrIrO_3$ by symmetry design, PNAS **116,** 16186 (2019).

[34] A. S. Patri, K. Hwang, H.-W. Lee, and Y. B. Kim, Theory of large intrinsic spin Hall effect in iridate semimetals, Sci. Rep. **8,** 8052 (2018).